Skin Color-Corrected Pulse Oximetry

Joel Kelsey, Max Melendez, Clarissa Pavao, Jack Roberts, and Professor George Gollin

University of Illinois-Urbana-Champaign

May 11, 2024

Abstract

Pulse oximeters have exhibited inaccuracies in measuring blood oxygen levels for individuals with darker skin tones, contributing to healthcare disparities based on race. This project aims to improve the commercial pulse oximeter to mitigate this bias, thereby improving the well-being and medical care for individuals with darker skin tones. This project investigates various methods of pulse oximetry utilizing a multi-wavelength spectrometer to measure the patient's skin tone. Additionally, the investigation focuses on using more than the standard two wavelengths (red and infrared light) to measure the blood oxygen levels accurately.

1 Introduction

Racial disparities in COVID-19 treatment reveal the long standing racial bias within contemporary pulse oximetry. Peripheral blood oxygen saturation (SpO_2) obtained from pulse oximeters are indirect measures of arterial blood oxygen saturation (SaO_2). Pulse oximeters would overestimate the blood oxygen saturation of black individuals by 1%, which is associated with lower admission rates and longer waits for treatment at hospital emergency departments [13]. In response to these disparities, this project's goal is to improve upon existing oximetry models, without drastically increasing the costs or ease of use, in order to assess the SpO_2 of patients with darker skin tones as reliably as lighter one. This racial bias has been in the medical community since the introduction of pulse oximetry, unrectified for decades.

Since its introduction in the 1980's, pulse oximetry has been integral to medical diagnostics, being both cheap and easy to use, so much so that the racial bias was ignored for decades [14]. However, a previous oximeter developed by HP–which was much more bulky and expensive–had rectified this problem in the 1970's using another technique [8]. Normal oximeters tend to use two wavelengths to measure blood oxygen: red and near-infrared. HP's model used five different wavelengths. Yet due to pulse oximetry's inexpensive nature, this

old "gold standard" fell out of use. Developing a method to combine pulse oximetry with HP's multi-wavelength method is the focus of this project.

2 Theory

Before the introduction of pulse oximetry, measuring SpO_2 involved some combination of invasive testing, expensive equipment, and difficult calibration. Even though the most accurate way to measure SpO_2 is through arterial blood gas tests, the procedure was invasive and expensive. From its inception, the goal of noninvasive oximetry has been to measure SpO_2 without the need to draw arterial blood. Early optical oximetry, developed at the tail end of World War II, used the Beer-Lambert law to distinguish between high and low SpO_2. The Beer-Lambert law relates optical attenuation to the concentrations of substances in a material. Not long after, the current standard of red and near-infrared light arose. This new kind of oximetry swapped the invasiveness of blood samples with the difficult calibrations of bio-optical measurements. It would take till the early 1980's to develop a cheap, easy to use technique: pulse oximetry.

Pulse oximetry utilizes a patient's pulse to distinguish between arterial blood and other parts of the body. This method supposedly could measure the substances in arterial blood while effectively excluding unwanted substance like skin, bone, and melanin. This proved to be untrue for numerous reasons, as will be discussed later. Developed at the same time as pulse oximeter, an eight wavelength oximeter designed by HP seemed to solve the skin color bias of oximetry's past. According to an article written in the October 1976 edition of the Hewlett-Packard Journal[8], their new oximeter had similar efficacy for both Black and non-Black patient.

2.1 The Beer-Lambert Law

Noninvasive oximetry starts with the Beer-Lambert law; it is basis for all subsequent noninvasive techniques. The Beer-Lambert law describes the relationship between the optical attenuation of light through a material and the absorption of that light by the concentrations of multiple substances in said material. Thus light transmitted through part of the human body, like an earlobe or a finger, is affected differently based on the concentration of substances.[7] The transmittance T of light through a material is related to its absorbance A (also known as optical density) as

$$\frac{I}{I_0} = T = 10^{-A}, \tag{1}$$

where I_0 is the intensity of the incident light, I is the attenuated intensity (i.e., the intensity of the light that made it through the material), and all quantities are dependent on the light's wavelength λ.

In the simplest case, when there is a single substance with uniform concentration, the Beer-Lambert law can be written as:

$$-\log T(\lambda) = A(\lambda) = l\varepsilon(\lambda)c, \tag{2}$$

where l is the optical path length (cm), c is the molar concentration of the substance (M), and ε is the absorptivity or extinction coefficient of the substance ($\text{cm}^{-1}\text{M}^{-1}$). This means that as either the concentration or extinction coefficient increases, more light is absorbed and the transmittance decreases. Since the extinction coefficient of substances are not necessarily equal at the same wavelength, materials can be distinguished by how there extinction coefficient change with wavelength. Once the material is known, its concentration can be derived.

The Beer-Lambert law for a material made of multiple substances states that the absorbance caused by each substance is linear. This is because each substance affects the transmittance independently and thus the absorbance in the exponent simply add together. However, it is important to note that the optical path length l, for each substance is not identical–each substances scatters light to different degrees. Therefore the more general formulation of the Beer-Lambert Law for m different substances is:

$$-\log T(\lambda) = A(\lambda) = \sum_{i=1}^{m} A_i(\lambda) = \sum_{i=1}^{m} \varepsilon_i(\lambda) \int_0^{l_i} c_i(z)\mathrm{d}z, \tag{3}$$

where ε_i, l_i, and c_i are the extinction coefficient, optical path length, and concentration of the i-th substance. Since oximetry requires a measurement of the absorbance at several wavelengths λ_k ($k = 1, 2, ...$), let $A_k = A(\lambda_k)$ and $\varepsilon_{k,i} = \varepsilon_i(\lambda_k)$.

For the purposes of oximetry, it is assumed that the material has minimal scattering and uniform concentrations, which means that the optical path length is the depth d of the material for all wavelengths. The difference in scattering can be assumed to be minimal because all the wavelengths are relatively close together, causing the optical path length to be approximately equal, having no effect on the final equation. Uniform concentrations can be assumed because using the average concentration over the optical path length does not change the total concentration of each substance. The simplified absorbance equation for the k-th wavelength can be written as:

$$A_k = d \sum_{i=1}^{m} \varepsilon_{k,i} c_i. \tag{4}$$

For decades, oximetry has used only two wavelengths–red (660 nm) and near-infrared (940 nm)–to measure SpO_2. This is because the extinction coefficients of oxygenated hemoglobin (HbO_2) and deoxygenated hemoglobin has easily distinguishable curves in that region, as shown in Figure 1. The algorithm used in most modern oximeters can be derived from the system of equations below. The Beer-Lambert equations for red and infrared with only oxygenated hemoglobin,

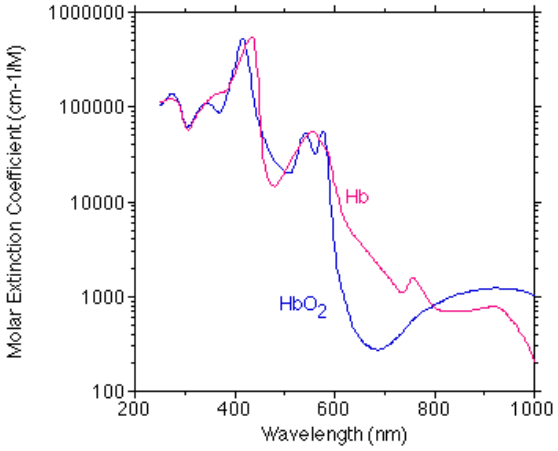

Figure 1: The change in the extinction coefficients of oxygenated and reduced hemoglobin for different wavelengths. Graph sourced from reference [11]

represented by o, and deoxygenated, represented by r, are:

$$A_R = d(\varepsilon_{R,o}c_o + \varepsilon_{R,r}c_r), \tag{5a}$$

$$A_{IR} = d(\varepsilon_{IR,o}c_o + \varepsilon_{IR,r}c_r), \tag{5b}$$

$$\beta \equiv A_R/A_{IR} = \frac{\varepsilon_{R,o}c_o + \varepsilon_{R,r}c_r}{\varepsilon_{IR,o}c_o + \varepsilon_{IR,r}c_r}. \tag{5c}$$

Since the path length is assumed to be the same for both wavelengths, an equation involving the absorbance ratio of two different wavelengths, denoted by β in Equation 5c, is not a function of that path length. The saturation of oxygenated and deoxygenated hemoglobin are represented by:

$$S_i = \frac{c_i}{c_o + c_r}, \tag{6a}$$

$$S_r = 1 - S_o. \tag{6b}$$

It is assumed that there is only the oxygenated and deoxygenated hemoglobin, meaning that the sum of their saturations is one. By replacing the hemoglobin concentrations in the ratio of attenuation equations (Equation 5) with the hemoglobin saturations (Equation 6a), reduced hemoglobin saturation can be substituted out using the sum of saturations in Equation 6b. Thus (after some algebra), the saturation of oxygenated hemoglobin can derived to be,

$$S_o = \frac{\varepsilon_{R,r} - \beta\varepsilon_{IR,r}}{(\varepsilon_{R,r} - \varepsilon_{R,o}) - \beta(\varepsilon_{IR,r} - \varepsilon_{IR,o})}, \tag{7}$$

which is only a function of the ratio of absorbances β.[12]

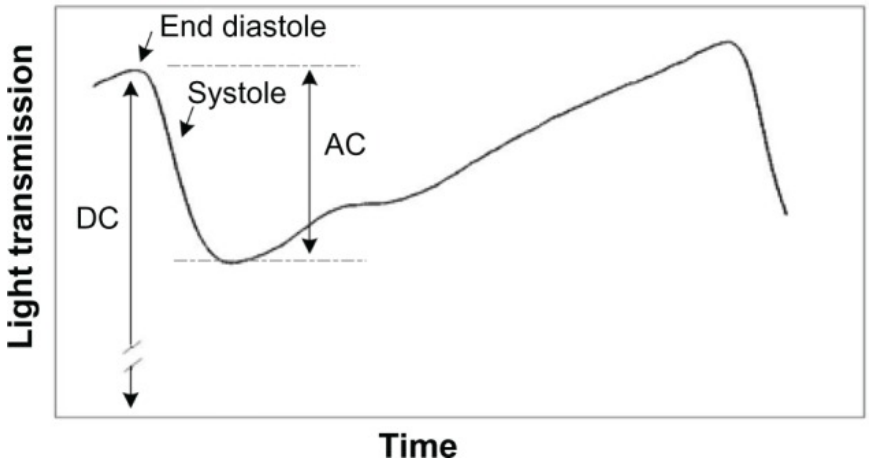

Figure 2: Example of the transmission signal for a single wavelength over the course of a single heartbeat. Sourced from reference [9]

2.2 Putting the "Pulse" in Pulse Oximetry

The pulse oximeter method was developed in the early 1980's. It utilizes the systole phase of the heart beat to attempt to measure only substances in arterial blood. The systole phase is when the heart contracts, pushing blood through out the body. This causes more blood to be pushed through extremities like fingers, resulting in the light transmission to precipitously drop from its maximum to its minimum. This periodic pattern can be measured and is assumed to be caused only by the change in volume of arterial blood caused by a heart beat. From this signal, two components are measured (as shown in Figure 2). The first measures the parts that are unchanging (e.g., skin, muscle, venous blood), which is when the light transmission is at its peak. Since it is supposed to not change, as opposed to the second, it is called the DC component. The second component measures the part that changes, assumed to be only arterial blood, which is the difference between the maximum and minimum caused by the systole phase. Since this component is the amplitude of the oscillation caused by the heart beat, it is called the AC component.

The ratio of the absorbances caused by the AC component and the DC component for a single wavelength is called the modulation ratio. This ratio has two purposes: separating the arterial blood from the rest of the substances in the human body and to cancel out the gain of the sensor used to measure the transmittance. If only the AC component was used, the oximeter would still need to be calibrated for each use. However, since the AC and DC components are measured using the same sensor, any gain caused by that sensor would be cancelled out by the modulation ratio. Thus instead of using the unmodulated absorbances in the β ratio, this modulated absorbance is used instead. There-

fore, pulse oximetry is a method that uses ratio-of-ratios of the form

$$R = \frac{A_{AC,R}}{A_{DC,R}} \Big/ \frac{A_{AC,IR}}{A_{DC,IR}} \,. \tag{8}$$

However using approach (Equation 8), instead of the simple ratio of absorption (Equation 5c), complicates the coefficients of the equation. The explicit extinction coefficients cannot be used to derive the equations coefficients. Instead, they must be found empirically for each pulse oximeter model.

$$S_o = \frac{1 - Rk_1}{k_2 - Rk_3} \tag{9}$$

Empirical studies must be performed by measuring SaO_2 and the transmittance read by the pulse oximeter at the same time. This data is then used to fit the coefficients of Equation 9 to create a reasonable approximation of blood oxygen saturation.

2.3 A Lost 'Golden Standard': Making a Multi-Ratio Pulse Oximeter

However, as pulse oximetry was being developed, a different method–a different machine–had been invented by HP. First released in 1977, HP's oximeter utilized 8 different wavelengths to measure the SpO_2 of the earlobe. By increasing the number of wavelengths used, more substances can be resolved, allowing for more accurate SpO_2 readings. By utilizing Kramer's method of solving systems of equations, HP was able to derive Equation 10, which is similar to the two wavelength version (Equation 9).

$$S_o = \frac{a_0 - \sum_{n=1}^{8} a_n A_n}{b_0 - \sum_{n=1}^{8} b_n A_n} \tag{10a}$$

$$A_n = -\log T_n \tag{10b}$$

$$0 = \sum_{n=1}^{8} a_n = \sum_{n=1}^{8} b_n \tag{10c}$$

However, it did not use even the simple ratio of absorbances. As such, HP's method for calibration was far less effective. To account for neutral density changes in transmittance, (i.e., any change which modifies all wavelengths equally), a boundary condition was set so that the sum of the absorbance coefficients equaled zero (as shown in Equation 10c). This resulted in the mathematical artifacts of a_0 and b_0. But, without the usage of the ratio-of-ratios, the machine had to be calibrated every 4 hours by measuring the light intensity without any absorbers present. The machine was also bulky, needing to utilize a rotating disc of light filters in order to measure all 8 wavelengths.

While HP's oximeter was considered the "gold standard" of oximetry[14], its bulk, cost, and occasional calibration meant that the smaller and inexpensive

pulse oximeter could become the predominate technique used. However, by re-deriving the equation HP used without the mathematical artifacts of a_0 and b_0, the $N+1$ multi-wavelength equation can be rewritten as

$$S_o = \frac{a_0 A_0 - \sum_{n=1}^{N} a_n A_n}{b_0 A_0 - \sum_{n=1}^{N} b_n A_n} \tag{11}$$

To reintroduce the ratios of absorbances, a reference wavelength, in this case the 0-th wavelength can be factored out in such a way as to make the first term of the numerator one (Equation 12a). This reintroduction of the absorbance ratios allows for the ratio-of-ratios for each wavelength (Equation 12b) to be used instead.

$$S_o = \frac{1 - \sum_{n=1}^{N} a_n R_n}{b_0 - \sum_{n=1}^{N} b_n R_n} \tag{12a}$$

$$R_n = \frac{A_{AC,n}}{A_{DC,n}} \Big/ \frac{A_{AC,NIR}}{A_{DC,NIR}} \tag{12b}$$

Equations 12 became the basis for the (> 2) multi-wavelength pulse oximeter developed during this project.

3 Methods

3.1 Overview

The new pulse oximeter design features two printed circuit boards interconnected by a ribbon cable. The first board is equipped with sensors, while the second is used to display the results. The display board is composed of an Adafruit Feather M4 Express along with an Adafruit wide angle TFT (Thin Film Transistor) LCD display with a microSD connector, an Adafruit DS3231 Precision RTC (Real Time Clock) sensor, and a ribbon cable connector. The sensor board consists of an Adafruit AS7341 11 Channel Light/Color Sensor, Spark Fun Pulse Oximeter & Heart Rate Monitor (MAX30101 & MAX32664), and a ribbon connector to attach to the display board. These two boards work together to measure, process, present blood oxygen levels and pulse rates.

3.2 Display Board Devices

From Figure 3, the Adafruit Feather M4 is the microcontroller responsible for data processing and management [4]. This device incorporates a built-in SD card slot for accessible data storage. Initially, the SD card serves as the primary method for data collection and analysis. Data are stored on the SD card, and blood oxygen levels are determined through Python analysis software. An alternative to this storage method is currently under development which will utilize software to run in real-time. This software will calculate the blood oxygen levels while the patient's finger is placed on the pulse oximeter device. This software will eliminate the need of data storage on the SD card.

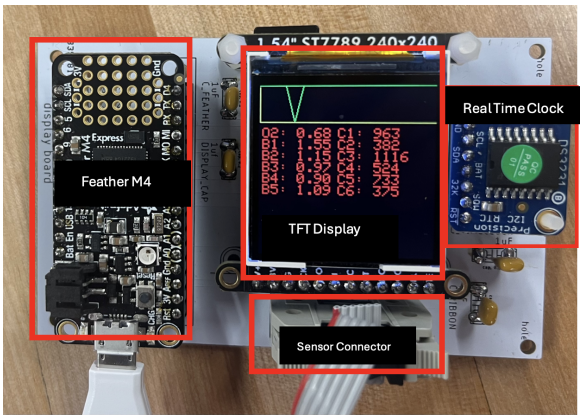

Figure 3: This figure shows the main display PCB board. It features the TFT LCD display, the Feather M4 Express, the RTC sensor, and the ribbon cable connector indicated by the red boxes.

The TFT serves as a visual interface, providing a comprehensive and clear color presentation of the results. The TFT shown in Figure 3 has 240 by 240 pixel display [1]. The design aims to display the blood oxygen levels and pulse rate on the screen in real time. The display shows the appearance of a pulse signal when a patient's finger is placed on sensor board, as indicated by the green graph on the top of the screen in Figure 3.

Below the green waveform of the pulse signal in the red text is the device reading out the SpO_2 values (denoted as O2), the channel number (denoted as C1, C2, C3, etc.), and the R values (denoted as B1, B2, B3, etc.). The SpO_2 is being calculated in real time; however, the readings do not yet match those of commercial pulse oximeters due to errors in the software described in a later section. This issue is fixable through correct calibration of the device using real arterial blood data from in-hospital tests. The channel numbers correspond to which wavelength channel of the spectrometer is being used at the time of data collection. A toy model was developed with toy data with toy data to find which combination of channels that would provide the most accurate blood oxygen measurements for all skin tones. The R coefficients purpose are described in the theory section of this paper. These values are the coefficients for the algorithm that calculates the blood oxygen values accurately for darker-skinned patients.

Including the RTC allows for precise timekeeping which is important since the signal we are trying to measure, a person's blood oxygenation and pulse rate, is changing over time. The Feather M4 has a built-in internal clock with millisecond accuracy. However, since this internal clock is not calibrated with an external real-time source, the RTC used in conjunction with the M4 enables tracking the time of each blood oxygen and pulse rate with millisecond precision. As mentioned previously, efforts are underway to to calculate the SpO_2 values in real time using the software. Upon successful implementation of this software,

integration of the RTC into data collection will proceed.

3.3 Sensor Board Devices

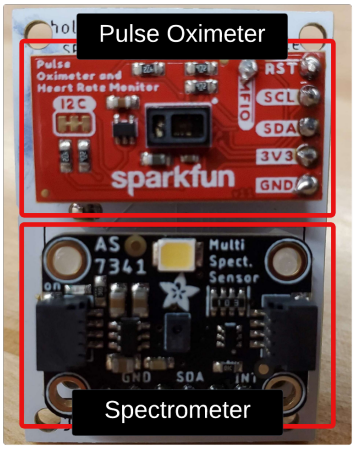

Figure 4: This figure shows the sensor board. It features the SparkFun Pulse Oximeter & Heart Rate Monitor and the Adafruit AS7341 11-Channel Spectrometer.

The AS7341 Light Sensor is designed to capture and interpret a broad spectrum of light. With 11 channels, this sensor enables detailed analysis of ambient light measurements and spectral analysis [2]. This sensor is small, only 3 x 2 mm footprint, but also includes sensors for white light as well as near infrared light [2]. This is where our device differs from the commercial pulse oximeter. The AS7341 gives access to 7 more wavelengths (445nm-680nm) than a commercial pulse oximeter. These additional wavelengths can be taken into account when doing the oxygen saturation calculation to accurately account for a patients skin color.

As mentioned in the theory section, more wavelengths than those used by the commercial pulse oximeter are required to determine the blood oxygen levels of darker-skinned patients. According to the data sheets of the AS7341 [3], control over which light channels to activate or deactivate has been established. Given the focus on only six of the wavelengths inside the spectrometer, as discussed previously in the Display Board Device section about using the toy model, the other five channels have been deactivated. This also helped with the sampling rate of the device. The speed of taking measurements has presented an obstacle. Isolating each component on both boards during measurements identified which parts were decelerating the overall process. It was discovered that the spectrometer was reconfiguring with each measurement taken. Allowing the spectrometer to continuously gather data without reconfiguring each time increased the speed

from 15 Hz to 28 Hz.

The future goal is to utilize the spectrometer to measure the six wavelength channels while simultaneously measuring the patient's pulse. This would eliminate the use of the Spark Fun pulse oximeter [10].

A pulse signal can be observed from the spectrometer. Results from trial runs are available in the Results section later in the paper. Using the MAX30101 as a heart rate monitor and the AS7341 for the blood oxygenation measurements improves the device's speed. Both measurements can be displayed on the TFT display as shown in Figure 3.

3.4 Printed Circuit Board

The PCB for both the display board and sensor board was was designed using EAGLE [6]. The placement of each breakout board was important as the accessibility to the microSD ports and battery ports needed to be open for easy use. See Figure 5 for the schematic of the main board.

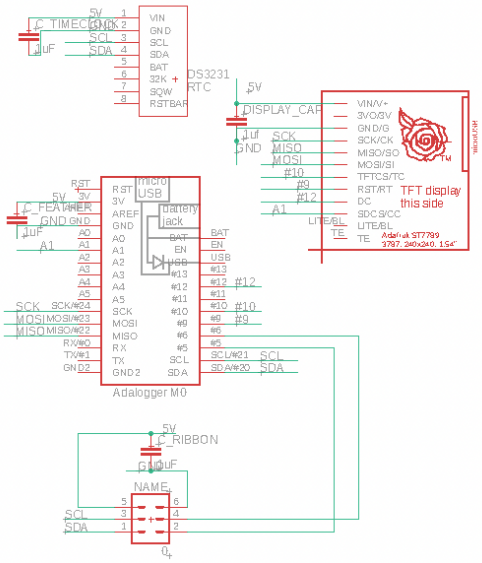

Figure 5: This figure shows the schematic from the EAGLE software of the main display board.

For the sensor board, a compact footprint was important, given its role in measuring a patient's physiological data through finger-based monitoring. See Figure 6 for the sensor board schematic layout. The two boards are connected with a ribbon cable so the measurements from the sensor board can be displayed and then recorded to the microSD on the display board.

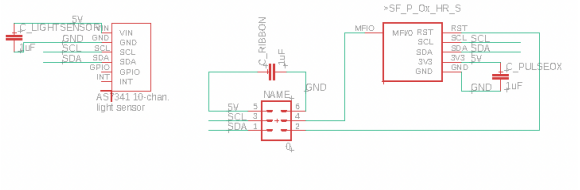

Figure 6: This figure shows the schematic from the EAGLE software of the sensor board.

3.5 3D-Printed Finger Case

In commercial pulse oximeters, a common design employs an alligator clamp mechanism, typically affixed to the patient's index finger, see Figure 8. In this project, the same clamp design was adopted to enable proper finger pressure on the sensors, ensuring consistent results. Optimal performance is contingent on maintaining a balance in pressure, as excessive or insufficient force on the sensors can compromise the accuracy of data acquisition. See the finger clamp CAD design in Figure 9. An example of what a pulse reading looks like if there is inconsistent pressure can be found in

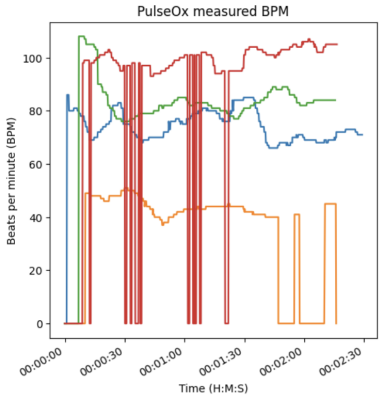

Figure 7: This figure shows an example of the a group of people doing a test run of their finger on the spectrometer and SparkFun pulse oximeter sensor. The x axis is the time and the y axis shows the beats per minute.

The red line in 7 shows what happens if a person does not keep proper pressure on the sensors. There are also dips in the orange line line data at the end as well. These large dips are when the sensor does not sense the finger and stops measuring. This is caused by inconsistent pressure and not enough pressure from the person being measured.

A case to cover the display board was also created for presentation purposes

and to not expose the sensors. See the CAD design for the display board in Figure 9. It must be noted that the clamp design shown in 9 was not used in most of the data collection in this paper. This is due to the fact that this design was not adopted until later into the project after the data analysis was complete.

Figure 8: This figure shows a commercial pulse oximeter. This design uses a clamp over the finger to measure the pulse and blood oxygenation levels of a patient.

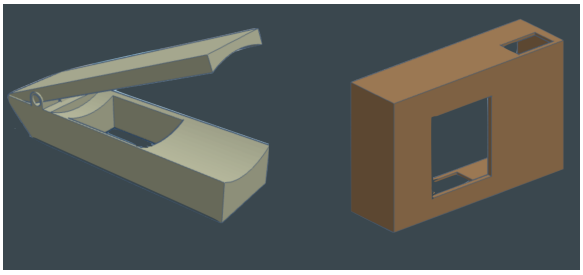

Figure 9: This figure shows the CAD designs of the finger clamp and display board cover.

3.6 Software

3.6.1 Software Overview

The software can be split into two major sections: an initialization setup and an operating loop. The initialization setup runs one time at the start of the code and the operating loop runs indefinitely or until the device is shut down.

Figure 10 provides a detailed description of the organization and workflow of the software. It begins with the initialization phase that runs through the

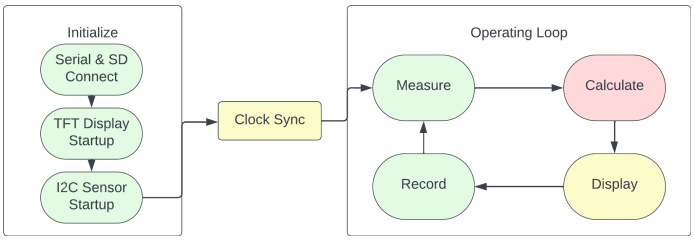

Figure 10: General organization of the software setup.

setup of the device. The serial & SD connect refer to the initialization of the C++ code and turning on the SD connection for data collection. Then the code starts up the TFT screen to display measurements. After initializing the TFT display, the code will prompt the I2C sensor (Inter-Integrated Circuit) to start.

Initialization is followed by a clock sync between the DS3231 real time clock and the Feather M4 internal timer. The DS3231 yields year/month/day/hour/second information and the Feather M4 yields millisecond information, with the two combined the data has timestamps down to the millisecond which can be used to take multiple data points a second. The clock sync will be further discussed later.

With the setup complete, the operating loop will run indefinitely. The operating loop takes a measurement, runs it through our peak-finding and SpO_2 algorithm, displays the readings on the TFT, and records the measurement to the SD card. This loop runs until the device is disconnected from power or the SD card is removed.

Device	**Library**	**Author**
DS3231	DS3231.h	Eric Ayars
All	SPI.h	Aurduino LLC.
All	Arduino.h	Aurduino LLC.
All	Wire.h	SparkFun Electronics
SD Card	SD.h	SparkFun Electronics
Pulse Oximeter	SparkFun Bio Sensor Hub Library.h	Adafruit
Spectrometer	Adafruit AS7341.h	Adafruit
TFT Display	Adafruit GFX.h	Adafruit
TFT Display	Adafruit ST7789.h	Adafruit

Table 1: Libraries imported within the initialization of the code.

The specific device functionalities are inside dedicated libraries written by the manufacturer. The specific libraries and which device they work with are shown in Table 1.

3.6.2 Initialization of Code

The initialization process, as depicted by Figure 11, begins with connecting the device to a computer over a serial connection with a baud rate of 115200. Next, the TFT display is connected using the SPI interface of the Feather M4. After this the I2C based devices, the Spark Fun pulse oximeter, the spectrometer, and the RTC, are connected to and setup. In order to increase the rate at which measurements are taken the I2C speed is then increased from standard mode (100 kbits / second) to fast mode (400 kbits / second).

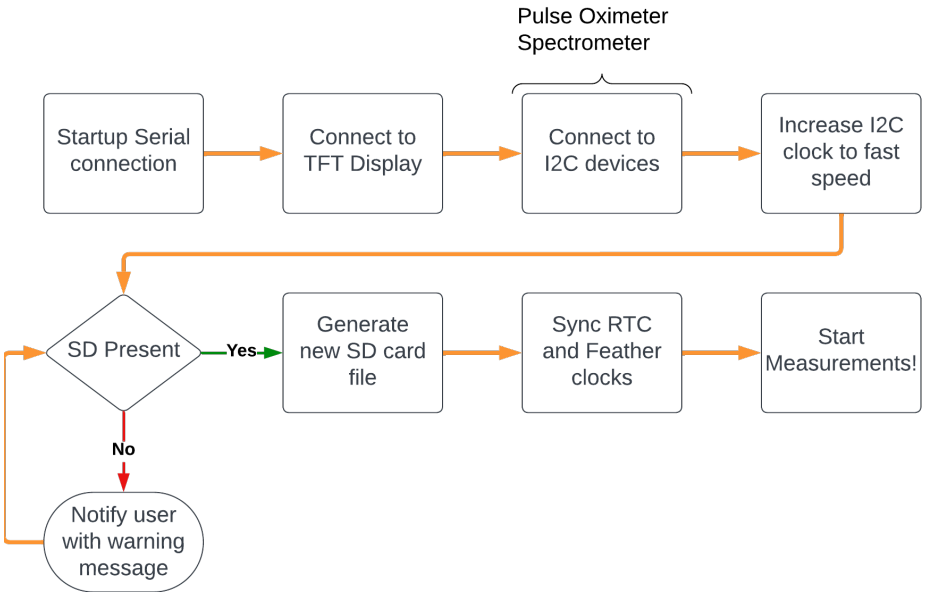

Figure 11: A diagram showing the initialization process of the device.

Once the communication rate is increased, the SD card attached to the Feather M4 is detected. If it is not present then the user is notified on both the TFT display and the serial connection. This continues until an SD card is detected. At which point a new data CSV file is created with columns for all I2C devices.

The final step in the initialization process is to sync the RTC with the internal clock of the Feather M4. This is done by waiting until the RTC has elapsed a single second. Once this happens the current value of the internal clock is recorded. This is used as an offset subtracted from the internal clock's value whenever it is recorded. This process makes it so the Feather M4's internal timer can record the milliseconds in between the RTC's second counts.

3.6.3 Operating Loop

A more detailed look at the operating loop can be seen in Figure 12.

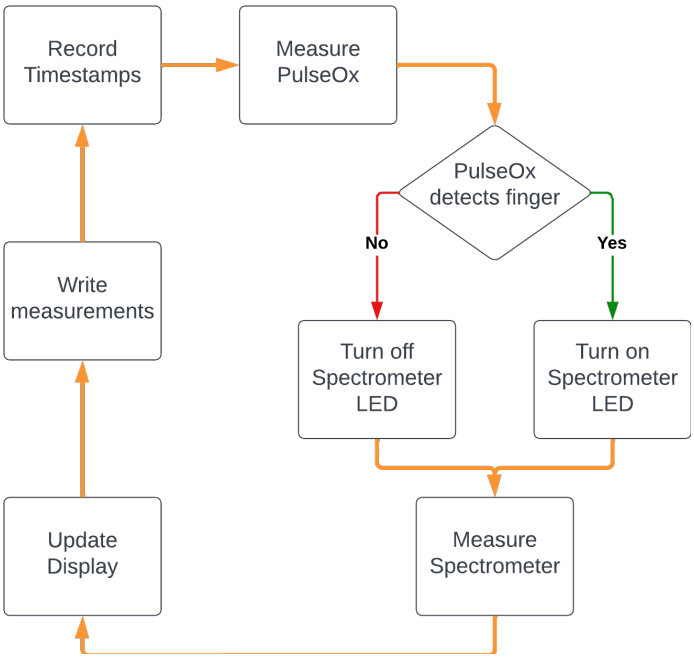

Figure 12: A block diagram of the operating loop of our device. The time stamps are intentionally taken as close to the measurements as possible to get accurate timing. The spectrometer has an LED which is turned on or off depending on the data from the Spark Fun pulse oximeter.

The primary operating loop is a sequential, but infinite loop that repeatedly takes data from the I2C devices as fast as possible while still updating the display. It begins by getting timestamps from both the RTC and the Feather's internal timer. Then the Spark Fun pulse oximeter and spectrometer are queried for data using their I2C interface. The data is used to update the display and write measurements to the CSV data file. At which point this loop now repeats.

3.7 Data Acquisition

In order to test the functionality of this device we need a standard experiment to acquire results from. In doing so, we can eliminate environment-related errors and make different measurements comparable.

To start, the patient places their left hand on the prototype with their pointer finger directly over the two sensors. Figure 13 shows an example of how the device was held during each of the experiments. Next their right pointer finger is put into a commercial pulse oximeter and monitored by a researcher. After a short verbal countdown, from the researcher, the prototype starts recording data and the oxygenation reported by the commercial pulse oximeter is manually recorded in ten second intervals. This recording process is done for a total of two

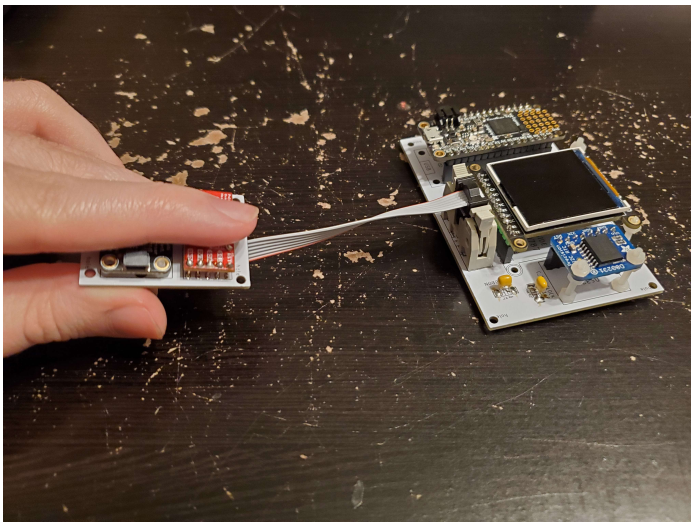

Figure 13: An example of how the device was held during each of the experiments

minutes. Once the time is up the prototype and commercial pulse oximeter are removed. The data from both is registered into comma separated value (CSV) data files to be analyzed later using python.

4 Results

4.1 Wavelength Counts

The raw data from the AS7341 spectrometer comes in the form of wavelength counts. Wavelength counts are an integer value proportional to the light intensity, at a specific wavelength, that are detected by the spectrometer. The two have a linear relationship, a higher number of wavelength counts means a higher light intensity.

An important distinction is that each measured wavelength is in reference to the center wavelength of that measurement channel. The AS7341 has 8 visible channels ranging from approximately 350-800 nm, channel 1 is centered at 415 nm, but has a full width half maximum value of 26 nm. In summary, while channels may be referred to as a specific wavelength they cover a small range of wavelengths.

Figure 14 is a representation of the measured wavelengths of the AS7341 normalized to the 680 nm channel. This is a visual representation of the center wavelength for each channel. Peaks occur at the center wavelength, but cover a greater range than the specific number.

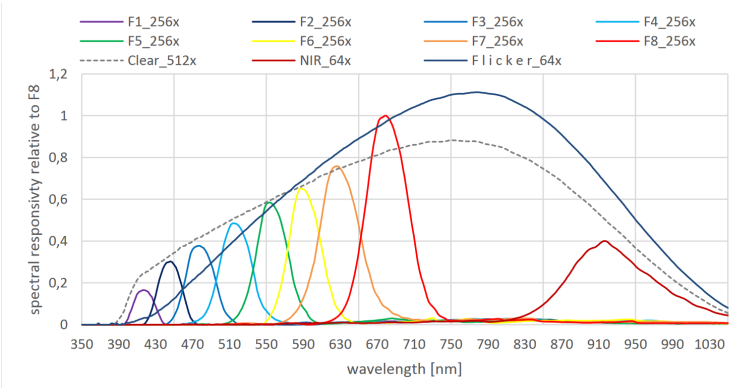

Figure 14: Measured spectral responsivity of the AS7341 relative to the 680 nm wavelength channel. [3]

4.2 Raw and Processed Data

The computation of the SpO_2 measurement begins with a reading of raw wavelength counts. These counts are then processed into ratios, as outlined the Section 2. The ratios become the driving force for SpO_2 calculation and are important to understand.

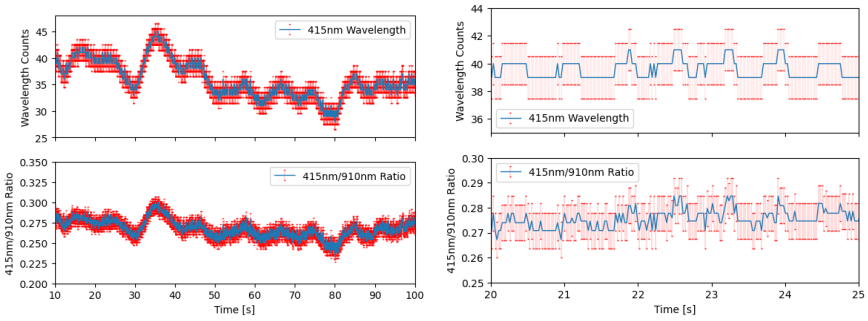

Figure 15: The top graphs show the raw counts of the 415 nm wavelength channel. The bottom graphs show the ratio of the 415 nm counts (Violet) over the 910 nm counts (Infrared). The left set shows the full dataset and the right set show a zoomed in 5 second time span. Error bars at set at 1 sigma to reflect full-width half-maximums given in the AS7341 Data sheet [2].

Figure 15 shows an example of some raw input data coming from the spectrometer. It also shows one of the ratios that is fed into the SpO2 algorithm (Bottom) described in Equation 12. Both have a clear oscillating nature to them.

The raw inputs need to be processes before inputting into the equations

described in section 1.2. To process these, an algorithm was designed that identifies highs and lows for the computed ratios. An example of this is shown in Figure 16.

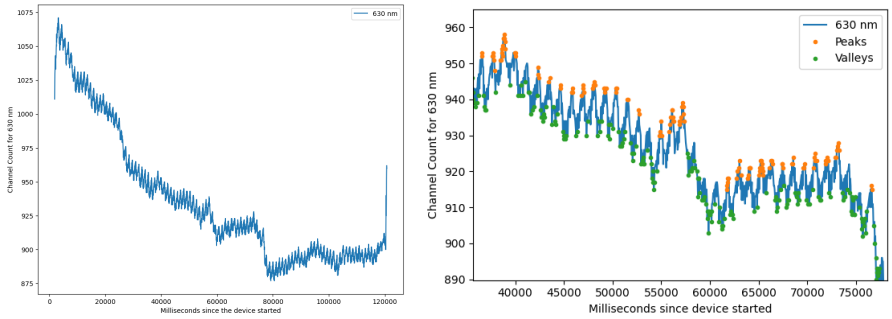

Figure 16: 630nm-930nm wavelength ratio plot (630nm/910nm). The left graph is the raw data of the ratios. The right graph is the ratios plot with the highs and lows marked by our peak recognition algorithm.

Properly identifying highs and lows is an extremely important part in the process of an accurate SpO_2 measurement. This step is crucial because it creates the input that will eventually lead to the final SpO_2 measure. The left graph in Figure 16 shows that the algorithm can sufficiently find peaks and valleys.

An important aspect of these ratios that contributes to more accurate results is the fact that all the peaks and valleys occur at the same time for every ratio. Each ratio has its own unique amplitudes and features, but all the peaks are at the same point in time. Using this fact, we can add all the ratios together and find the peaks and valleys on the sum of all the ratios. This leaves us with a timestamp for all the peaks and valleys, it also ensures a peak won't be recognised at one wavelength and not the others.

With the ratio amplitudes clearly defined, they can now be fed into our SpO_2 algorithm to get the final result. The SpO_2 algorithm still requires fine tuning, it needs to be trained off real world data to get an accurate reading. This will be the final step and give us the desired blood-oxygen reading

4.3 Light Characterization

In order to best understand the functionality of the spectrometer a detailed and accurate spectrum of the light source is needed. On the AS7341 board itself is the EAHC2835WD6 white LED from Everlight Electronics [2] which has a documented ranges of spectra that could occur. The variation in spectrum is a result of the manufacturing process and cannot be controlled by the device. Initially we set out to recreate this spectrum with the AS7341 itself. This was accomplished by placing two AS7341 boards facing towards each other. The first board had a singular purpose of providing illumination while the second was taking measurements of all of its channels. This was measured for approx-

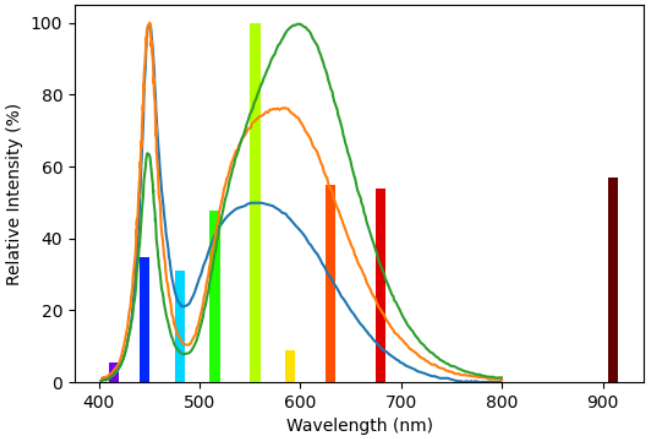

Figure 17: A comparison of the relative intensity measured by the AS7341 and predicted by the manufacturer's documentation. The bars indicate the measurement while the lines are from the documentation. The two anomalies are in the 590 nm channel and the 910 nm channel. The first of which is lower than expected and the other is not expected to occur.

imately a minute. The time averaged measured spectrum is shown in Figure 17 and generally shows good agreement between the expected spectrum and measurements.

The main concern as a part of this plot is the source of the NIR component as it does not seem to be documented by the manufacturer's of the LED. This will be discussed in a later section but the NIR component we are observing does not have a known source and likely is a form of noise in our system.

4.4 SpO_2 Fits

Using the data that was acquired from the commercial pulse oximeter and our device we could perform a series of curve fittings attempting to characterize the relationship between the ratio of ratios and the SpO_2. This fit was done with the Gauss-Newton algorithm and an analytical Jacobian of the algorithm described in the theory section. Since there could be timing differences between the commercial pulse oximeter and our device a linear interpolation was performed to get likely values between known measurements.

Combining all of the peak data that was previously calculated a total of 8 people were measured according to the above procedure. Within these signals, a total of 962 peaks were found and their corresponding SpO_2 was used in the fitting method. Two example SpO_2 measurements are depicted in Figure 18.

In order to evaluate the effectiveness of the SpO_2 regression a good comparison between the predicted and known SpO_2 values is required. This was

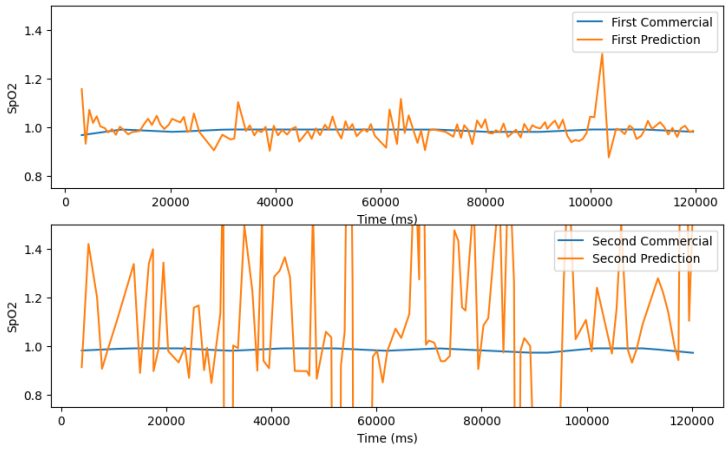

Figure 18: An example of the variance in the predictions of our model over time. In the top graph the overall prediction is quite similar to the commercial pulse oximeter. At the same time a different patient seemingly is not estimated very well by this model.

approached by creating a scatter plot comparing the two, as shown in Figure 19. By plotting the commercially measure values along the x-axis and the predicted values along the y-axis a general relationship between the two can be visualized. If our fit reproduced exactly the measured values then there would be a linear relationship between the two with a slope of 1. In Figure 19, there does appear to be a linear relationship between the two with the cluster in the range from 0.8 to 1.2 predicted SpO_2. However, this linear relationship appears to have significant variance from this cluster especially towards the high commercial SpO_2 range. In addition, the slope is negative suggesting that the fit tends to overestimate at lower SpO_2 values relative to the commercial pulse oximeter. This suggests that the current fitting technique is ill posed and/or incomplete. This is supported empirically by the results of this analysis being highly dependent on the initial values of the model's coefficients. One potential method to get a better fit would be to apply a set of constraints onto the coefficients. Doing so might enable the use of techniques typically applied to fractional linear programming, a type of optimization problem. More work needs to be done to fully assess what regression technique would work best for this kind of problem.

5 Discussion

5.1 Missing Infrared Component in the AS7341 LED

Through initial testing, the AS7341 LED appears to contain some infrared component. Routine testing yielded approximately 100 wavelength counts per mea-

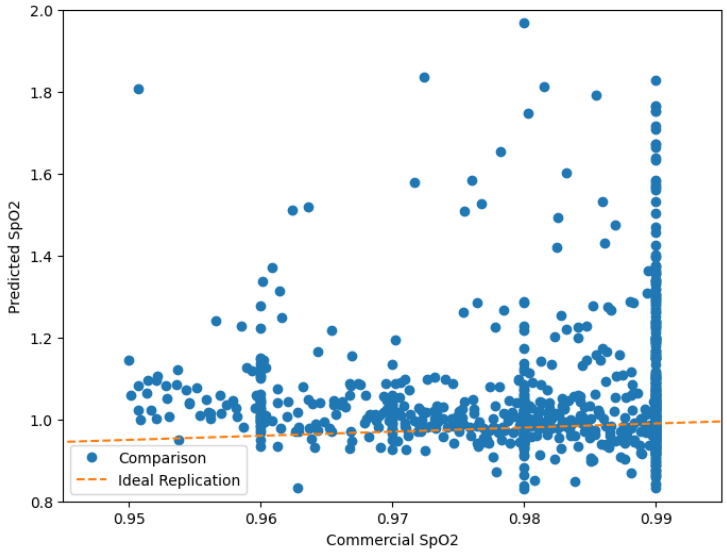

Figure 19: A scatter plot depicting the relationship between the predicted and the commercially measured SpO_2 values. It does appear like there is a linear relationship but it appears to have a near-zero negative slope. There is additionally quite a bit of noise to these predictions suggesting that the device's noise is drastically affecting performance. The clustering on the x-axis at particular values is due to the commercially measured SpO_2 having little variance over the two minute duration. This leads to the interpolated value having little or no change over some intervals leading to repeated x values.

surement and the values appeared to have modulation. As testing continued, the source of the infrared component became unclear and the need for an addition infrared (IR) LED became apparent.

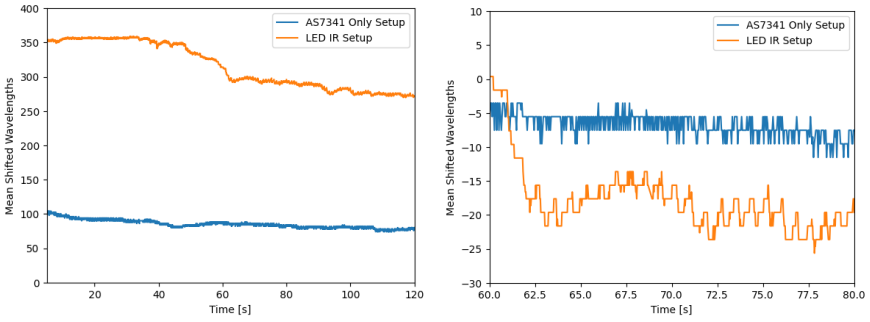

Figure 20: Comparison between the device with an added infrared LED and the device using only the AS7341 LED. The left graph shows unaltered wavelength counts for both setups. The right graph shows both measurements shifted by their means to compare the amplitude of their modulation.

Figure 20 shows the comparison between the device with and without the additional IR LED. At the magnitude of the IR LED measurement, the old setup displays no modulation. In the right graph of Figure 20, the wavelength counts of the IR LED setup are almost three times larger than that of the old setup.

Looking at the left graph in Figure 20, the AS7341 only setup stays along a generally straight path with modulations that appear to be noise. The LED IR Setup, shows much clearer modulation that is much more similar to the theoretical curve in Figure 2.

Using a Thorlabs CCS200/M - Compact Spectrometer (Extended Range: 200 - 1000 nm), we took measurements further to characterize the AS7341's LED. This gives us the ability to take measurements with an outside source, instead of using another AS7341.

Figure 21 shows the results of the the AS7341 LED with the Thorlabs CCS200/M. The left graph in Figure 21 shows a maximum intensity around 600 nm, and a near-zero intensity from 200-400 nm and 850-1000 nm. The right graph in Figure 21 gives a closer look at the 900-1000 nm wavelength range, here we have an average relative intensity of 0.02264. The infrared component is the most important of any of the wavelengths because many of the ratios, described in the Theory section, use the infrared component as their denominator. For these reasons, the AS7341 LED is insufficient and the addition of an IR LED was deemed necessary for out setup.

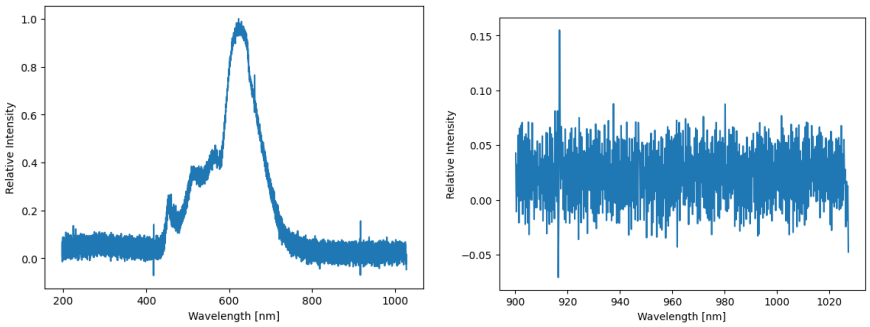

Figure 21: Data taken on the AS7341 LED using the Thorlabs CCS200/M - Compact Spectrometer. Intensity is relative to the maximum intensity value.

5.2 Clock Sync

The clock sync is the product of the DS3231 not having millisecond information, it only provides seconds, minutes, hours, day, month, and year information. Because this devices records multiple measurements per second, it requires the utilization of the Feather M4's millisecond timer to get the exact time of a measurement. Syncing the timers up so the Feather M4 is recording the milliseconds between each DS3231 second is the purpose of this point in the software.

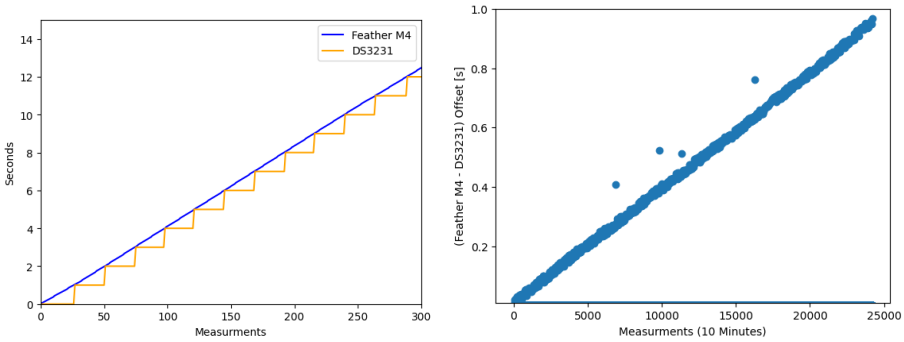

Figure 22: Display of the DS3231 and Feather M4 timing resolutions and offset. The left shows the beginning of the measurement, when the timers are perfectly in sync. The right shows the difference between the two timers over a 10-minute measurement.

Figure 22 shows a graphical representation of the time sync. The left graph shows perfect agreement between the DS3231 and the Feather M4 at the beginning of a measurement. As time goes on, a slight difference between the two measurements begins to arise. In a 110 second measurement, the Feather M4 leads the DS3231 by 0.194 seconds. Over the course of a ten minute measurement, the Feather M4 leads by almost a whole second.

Judging off these measurements, this produces an offset of 0.0017636 seconds every one second that passes. While this uncertainty is fairly small, it does pose a source of error within our device at long time scales. For the current use cases of our device, measurements rarely exceed that of the two-minute measurement described in Section 3.7. Under these circumstances, the 0.194 second offset does not pose significant issues for our measurements and is within usable error. This aspect of the timing system will need to be further developed if the device were to be used at longer timescales, such as overnight on a patient at a hospital.

5.3 Displacement From Sensor

A point in testing was whether or not displacement from the finger and the color sensor had a significant impact on the readings of our device. This could have impacts in terms of fabrication for a housing and methods of measurements so it would be important to take data on both cases.

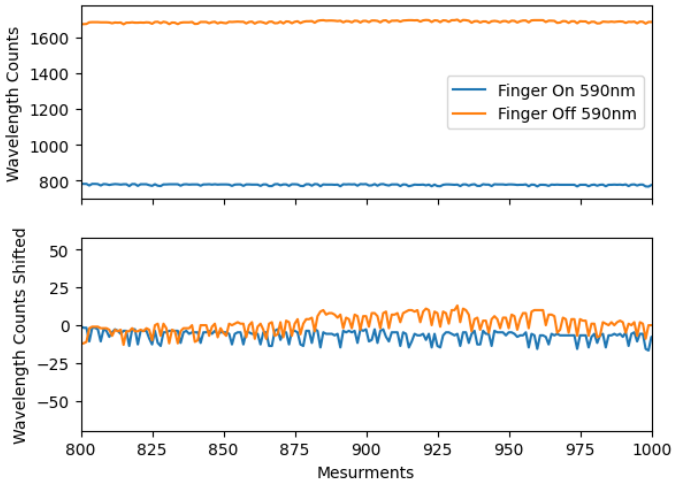

Figure 23: The top graph shows the raw data of the finger on the sensor (Finger On 590nm) and the finger lifted off the sensor by approximately 2mm (Finger Off 590nm) at the 590nm wavelength. The bottom graph shows the two measures shifted by their means. Both are graphed as counts at the 590nm wavelength with the number of measurements on the x-axis.

Looking at the top graph on Figure 23 it is clear there are significantly more wavelength counts when the finger is elevated from the sensor compared to when it is pressed against the sensor. This is likely due to lights outside the system, like those in the room, bleeding into the measurement which is supported by testing in a dark environment that resulted in a more similar magnitude when compared to the finger pressed on. When we shift both to zero, by subtracting their means, they become more similar. The finger off still exhibits an oscillatory nature similar to the finger on. As the measurements can't be taken at the same

time, we can't compare exact points. We can, however, take a Fourier transform to find what frequencies dominate the measurements and compare those.

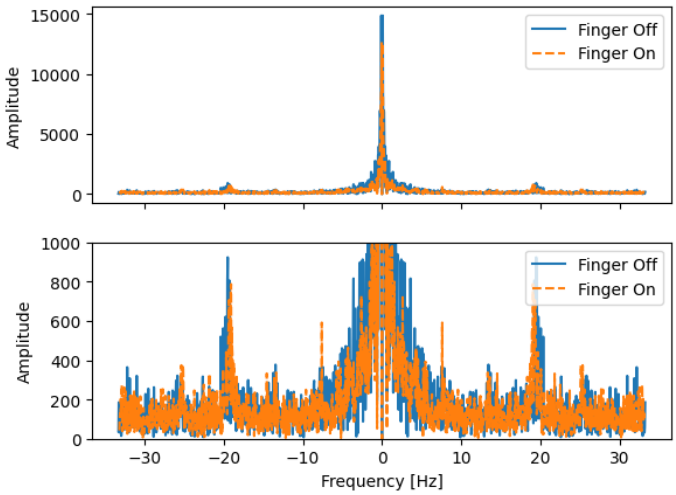

Figure 24: Computed Fourier transform mean shifted data of the finger on the sensor (On) and the finger lifted off the sensor by approximately 2mm (off) at the 590nm wavelength. The top is the whole transform and the bottom is a closer look at the bottom of the peak.

When the Fourier transform is computed for each case, a clear difference in amplitude arises. The finger off case has a much higher amplitude than the finger on. We can surmise more by taking a closer look at the base of the peak in the bottom graph on Figure 24.

Looking at the transforms close up, it becomes obvious that the 'finger off' displays a lot more noise than the 'finger on'. They still exhibit similarities between each other, but the noise is significant. Both display a peak at the frequency of approximately 20 Hz, which is in line with our expectations as the average sampling rate for these tests was approximately 22.5 Hz. Again, we do see a higher peak from the 'finger off' case which is likely due to outside noise. Taking a look at the data along the bottom and near the base of the 0 Hz peak, there is another example of additional noise from the 'finger off' case.

Between the disparity in amplitude and the added noise, it was determined the finger displacement introduces additional systematic effects in the recorded data and should be avoided if possible.

5.4 Sampling Rate

The sampling rate of the device is important to accurately recreate an analog signal the measurement frequency needs to be at least twice that of the maximum signal frequency by the Nyquist-Shannon sampling theorem [5], this means

we require upwards of 30 measurements per second. Initial versions of our code only had 5 measurements per second when the spectrometer, pulse-ox, and TFT display were all running at the same time.

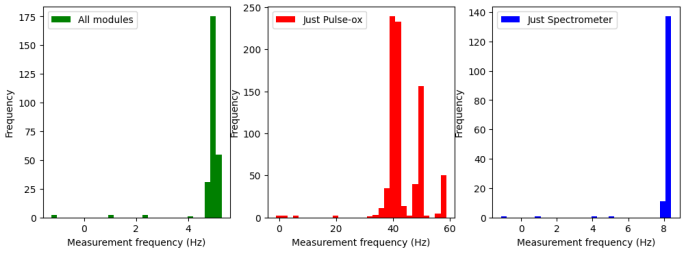

Figure 25: Measurement frequency graphs for each of the main modules of our device in an early form of our code.

Figure 25 shows the sampling rate of all components, the pulse-ox, and the spectrometer in an early version of the code. The "All Modules" histogram also includes the TFT Display which runs even slower than the spectrometer's 8 Hz. Because all the components rely on each other for each measurement, one component being slower than another can create a bottleneck for the whole process. Referring back to the operating loop diagram in Figure 12, the loop is only as fast as each of the steps. The pulse-ox is fast enough on its own, but the spectrometer would need to be significantly increased to satisfy the Nyquist-Shannon sampling theorem. This lead to alterations to the integration speed on the spectrometer. Integration time corresponds to the how long the spectrometer is taking in photons to make a measurement, this can correlate to improved signal-to-noise ratio if maximized. For the AS7341, this integration time is controlled by two factors: ASTEP and ATIME. These factors are combine in the following equation:

$$\text{Integration Time} = (\text{ATIME} + 1) * (\text{ASTEP} + 1) * 2.78\mu S \tag{13}$$

Altering this equation can speed up or slow down the length of time measurements taken on the AS7341.

Figure 26 shows the change of integration time in action, especially when compared to Figure 25 where the spectrometer had ASTEP = ATIME = 100. These changes are not linear, while the jump from 50-50 to 25-25 yields 4-5 measurements, the jump to 10-10 only yields 1. This is likely because ASTEP = ATIME = 10 is nearing the maximum sample frequency of the AS7341, while it theoretically goes to 2.78 μS at ASTEP = ATIME = 0 that won't actually be the case in practice. In addition, the lower we go on integration time, the more room we open up to noise. It's important to keep the downsides in mind when setting ASTEP and ATIME which is why we typically fall between 50-100 for these values.

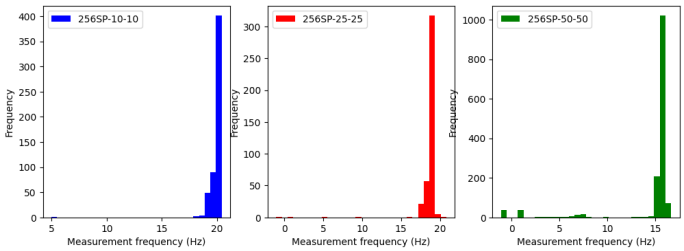

Figure 26: Measurement frequency histograms of the spectrometer for ASTEP-ATIME: 10-10, 25-25, 50-50.

5.5 Future Plans

The primary place for future improvements will be finding values for the coefficients in the algorithm obtained from a hospital blood gas test. The blood gas test will provide the correct coefficients to calibrate the device. Currently, the calibration coefficients are being used from the toy data described in the Display Board Devices section. The blood gas test will replace those toy values with the actual coefficients.

Another improvement is in the development of the prototype version two PCB. This version mainly consists of small improvements such as pin hole adjustments and fixing small errors the first board had. Consideration is also being given to using a smaller TFT display in the next prototype. As the two PCB's are being used together, tracking of any additional changes that can improve efficiency is ongoing.

As for software, plans include correcting time syncing issues between the RTC and the Feather M4 internal clock. The speed of the Spark-Fun pulse oximeter and the spectrometer needs to increase. Implementation of software to increase the speed of data collection is underway, which will improve our accuracy.

6 Conclusion

This paper presents the current plans and developments in updating the commonly used pulse oximeter using a hybrid of methods of using five additional wavelengths of light and a ratio of those wavelengths to accurately calculate the blood oxygenation of darker-skinned patients. The relevant inaccuracy of commercial pulse oximeters, as presented in the literature, has been recognized. This project's plan includes exploring a wider range of wavelengths to observe the absorbance, reflectance, and transmittance of a finger to measure the blood oxygen levels. In addition to the increased number of wavelengths, which will be measured with the spectrometer, the Spark-Fun Pulse Oximeter & Heart Rate Monitor has also been implemented to compare results.

A custom algorithm has been implemented which takes into account the

larger number of measured wavelengths. This algorithm has coefficients that allow accurate measurements the blood oxygenation of dark-skinned patients. It functions for the two PCBs connected with a ribbon cable connector; one board displays and stores measurements, while the other takes measurements. Minor adjustments are being made to improve the efficiency and layout of the PCB design. Additionally, a finger clamp was created to improve the results from the Spark Fun pulse oximeter across all subjects. Overall the abilities of this prototype are unclear due to the issues involving the fit between the commercially measured pulse oximetry values and the ratio of modulation ratios measured from the spectrometer. There does appear to be a linear relationship between the given values and predicted values however, the prediction has a significantly high variance from the assumed value. This is likely due to the fitting process being ill posed. Thereby, more investigation into this technique and the proper mathematical tools needed for this analysis. Even without the algorithmic prediction fully functioning it is clear that the type of light source used in devices like these has a large impact on the abilities of the device itself, even if more types of light are taken into account.

7 Acknowledgements

We would like to thank the project staff: George Gollin, Yuk Tung Liu, and Shengzhu Yin.

References

[1] *Adafruit 1.3″240x240 Wide Angle IPS TFT Display*. Retrieved 14 Novemeber, 2023 from https://www.adafruit.com/product/4313. 2023.

[2] *Adafruit AS7341 10-Channel Light / Color Sensor Breakout - STEMMA QT / Qwiic*. Retrieved 14 Novemeber, 2023 from https://www.adafruit.com/product/4698. 2007.

[3] *Adafruit AS7341 Library*. Retrieved 2 April, 2024 from https://adafruit.github.io/Adafruit$_A$S7341/*html*/ 2007.

[4] *Adafruit Feather M0 Basic Proto - ATSAMD21 Cortex M0*. Retrieved 10 Novemeber, 2023 from https://www.adafruit.com/product/2772. 2007.

[5] NATIONAL INSTRUMENTS CORP. *Nyquist and Shannon's Sampling Theorems*. Retrieved 8 May, 2024 from https://www.ni.com/docs/en-US/bundle/ni-fgen/page/nyquist-and-shannons-sampling-theorems.html. 2023.

[6] AutoDesk Fusion Inc. *EAGLE AutoDesk Fusion*. Retrieved 8 May, 2024 from https://www.autodesk.com/products/eagle/overview?term=1-YEARtab=subscription. 2023.

[7] Steven L Jacques. "Optical properties of biological tissues: a review". In: *Physics in Medicine Biology* 58.11 (May 2013), R37. DOI: 10.1088/0031-9155/58/11/R37. URL: https://dx.doi.org/10.1088/0031-9155/58/11/R37.

[8] Edwin B. Merrick and Thomas J. Hayes. "Continuous, Non-invasive Measurements of Arterial Blood Oxygen Levels". In: *Hewlett-Packard Journal* (Oct. 1976), pp. 2–10. URL: http://www.rsp-italy.it/Electronics/Magazines/HP%20Journal/1976-10.pdf.

[9] Meir Nitzan, Ayal Romem, and Robert Koppel. "Pulse oximetry: Fundamentals and technology update". In: *Medical devices (Auckland, N.Z.)* 7 (July 2014), pp. 231–9. DOI: 10.2147/MDER.S47319.

[10] *parkFun Pulse Oximeter and Heart Rate Sensor - MAX30101 & MAX32664 (Qwiic)*. Retrieved 14 Novemeber, 2023 from https://www.sparkfun.com/products/15219. 2007.

[11] Scott Prahl. *Optical absorption of hemoglobin*. 1999. URL: https://omlc.org/spectra/hemoglobin/index.html.

[12] K.J. REYNOLDS et al. "TEMPERATURE DEPENDENCE OF LED AND ITS THEORETICAL EFFECT ON PULSE OXIMETRY". In: *British Journal of Anaesthesia* 67.5 (1991), pp. 638–643. ISSN: 0007-0912. DOI: https://doi.org/10.1093/bja/67.5.638. URL: https://www.sciencedirect.com/science/article/pii/S0007091217478913.

[13] Sylvia E K Sudat et al. "Racial Disparities in Pulse Oximeter Device Inaccuracy and Estimated Clinical Impact on COVID-19 Treatment Course". In: *American Journal of Epidemiology* 192.5 (Sept. 2022), pp. 703–713. ISSN: 0002-9262. DOI: 10.1093/aje/kwac164. eprint: https://academic.oup.com/aje/article-pdf/192/5/703/50327279/kwac164.pdf. URL: https://doi.org/10.1093/aje/kwac164.

[14] Michael W Wukitsch et al. "Pulse oximetry: analysis of theory, technology, and practice". In: *Journal of clinical monitoring* 4 (1988), pp. 290–301.